

1 Article

2 Pulse Current of Multi-needle Negative Corona 3 Discharge and its Electromagnetic Radiation 4 Characteristics

5 Chuang Wang, Xi Chen*, Jiting Ouyang and Jialu Fu

6 State Key Laboratory of Mechatronics Engineering and Control, Beijing Institute of Technology,
7 Beijing 100081, China; cunghens@163.com (C.W.); jtouyang@bit.edu.cn (J.O); luvivid@163.com (J.F.);

8 * Correspondence: chenxi@bit.edu.cn (X.C.); Tel.: +86-010-6891-8017

9

10

11 **Featured Application:** Authors are encouraged to provide a concise description of the specific
12 application or a potential application of the work. This section is not mandatory.

13 **Abstract:** Negative corona discharges occur widely in high voltage transmission lines and charged
14 aircraft, which can cause strong electromagnetic interference. Negative corona discharge is typically
15 performed simultaneously at multiple discharge points. In this study, the current and its EM
16 radiation characteristics of single-needle and multi-needle negative corona discharge in different
17 conditions were tested. The current and electromagnetic radiation characteristics of the two
18 discharge structures were compared. The dipole radiation model was established to analyze the EM
19 radiation characteristics of the negative corona discharge. The results show that, It is only when the
20 voltage reaches a certain threshold that the current and electromagnetic radiation fields of the multi-
21 needle discharge structure will be superimposed and their amplitudes will increase significantly.
22 The frequency of electromagnetic radiation signal does not change with the number of needles,
23 cathode geometry and applied voltage, but only depends on ambient pressure. It provides a basis
24 for detecting corona discharge sources under different conditions.

25 **Keywords:** corona discharge; Trichel pulse; multi-needle; EM radiation

26

27 1. Introduction

28 Corona discharge is a relatively low-energy discharge process that occurs only in a strong
29 electric field near a small radius of curvature electrode[1,2]. Corona discharge is a common discharge
30 phenomenon, which occurs in plasma generator, ozone generator, electrostatic precipitator,
31 electrostatic printing, electrostatic charge of aerosol particles, high voltage transmission lines and
32 charged aircraft[3–10]. Corona discharge is usually performed simultaneously in a multi-needle
33 (multi-point) format[6,8,11]. Corona discharge is divided into positive corona discharge and negative
34 corona discharge according to the difference of the electrode polarity of the small curvature radius in
35 the discharge structure. Negative corona discharge currents exhibit a regular pulse form, called
36 Trichel pulse[12], which can cause strong EM interference. On the one hand, multi-needle negative
37 corona discharge can cause the loss of power high voltage equipment, radio interference and
38 television interference[13]. On the other hand, multi-needle negative corona discharge
39 electromagnetic radiation signals can be used as target signals for high-voltage transmission line
40 detection and high-altitude aircraft target recognition[14].

41 Corona discharge and its EM radiation characteristics have always been the focus of research.
42 Juette [15] tested the EM interference near 75 high-voltage lines under different weather conditions.
43 On this basis, S.K Nayak[16] and others in India established a preliminary calculation model for

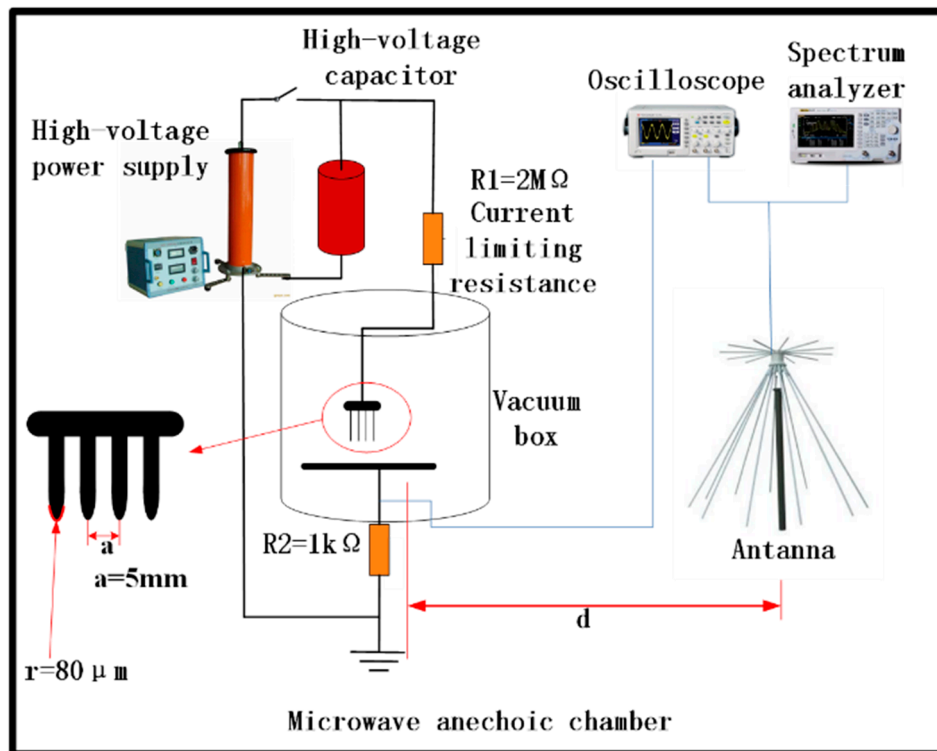
44 corona current pulses and calculated the corona radiation interference in high-voltage transmission
45 lines. However, these studies did not rule out the effects of partial discharges such as spark
46 discharges, so the test results were not accurate enough. Yasuyuki T et al[17]. experimentally studied
47 the spectrum of the negative corona discharge radiation signal under the needle-plate discharge
48 structure and compared it with the spark discharge EM radiation signal. Although they obtained the
49 spectrum of the negative corona radiation signal, they did not analyze the mechanism of the radiation
50 signal. Zhang Yu[18] et al. studied the relationship between the spectrum of the single-needle
51 negative corona radiation signal and the discharge parameters and believed that the spectrum of the
52 discharge EM radiation signal is only related to the rising time of the Trichel pulse current. But the
53 study did not analyze the discharge EM radiation process. In addition, the above studies did not pay
54 attention to the EM radiation characteristics of multi-needle discharge. The corona discharge on the
55 high-voltage transmission line is often multi-point simultaneous discharge, and the EM radiation
56 characteristics of multi-point and single-point corona discharge are significantly different. At present,
57 researches on multi-needle (multi-point) discharge mainly focus on the volt-ampere characteristics
58 of discharge and the interaction analysis of discharge process. Researches on the superposition of the
59 multi-needle negative corona discharge Trichel pulse current and the interference of the discharge
60 EM radiation signal are rare.

61 In this paper, the current characteristics of multi-needle negative corona discharge and its EM
62 radiation characteristics were studied. A test system for negative corona discharge radiation
63 characteristic was set up. The effects of discharge parameters on the single-needle negative corona
64 discharge Trichel pulse current and its EM radiation field were tested. The current superposition of
65 multi-needle negative corona discharge and the interference of the EM radiation field were studied.
66 The EM radiation model of dipole negative corona discharge was established, and the relationship
67 between the EM radiation characteristics of negative corona discharge and the parameters of the
68 discharge system was analyzed. This study can provide a reference for corona discharge detection of
69 high-voltage transmission lines.

70 2. Experimental Setup

71 The experimental system is shown in Figure 1, which consists of a high voltage generating
72 module, a discharging module, a signal detection module and a shielding module. The high voltage
73 generating module includes the high voltage power supply and the high voltage capacitor. During
74 the experiment, the high voltage power supply first charges the high voltage capacitor. The high
75 voltage power supply is turned off when the voltage reaches a predetermined value. The use of the
76 high voltage capacitor to supply the discharge needle can eliminate the EM radiation interference
77 generated by the high voltage power supply. The capacitance is 20 μf and the withstand voltage is 20
78 kV. The discharging module includes a discharge needle, a grounding plate, a displacement platform
79 and a vacuum box. Discharge experiments of discharge needles of different tip radius can be carried
80 out through the change of the discharge needle, and multi-needle simultaneous discharge
81 experiments can also be performed. The displacement platform can be used to precisely control the
82 gap of the electrodes. The vacuum box can control the air pressure of the discharge environment. The
83 grounding plate is grounded through a 1 k Ω sampling resistor.

84



85 **Figure 1.** Experimental setup

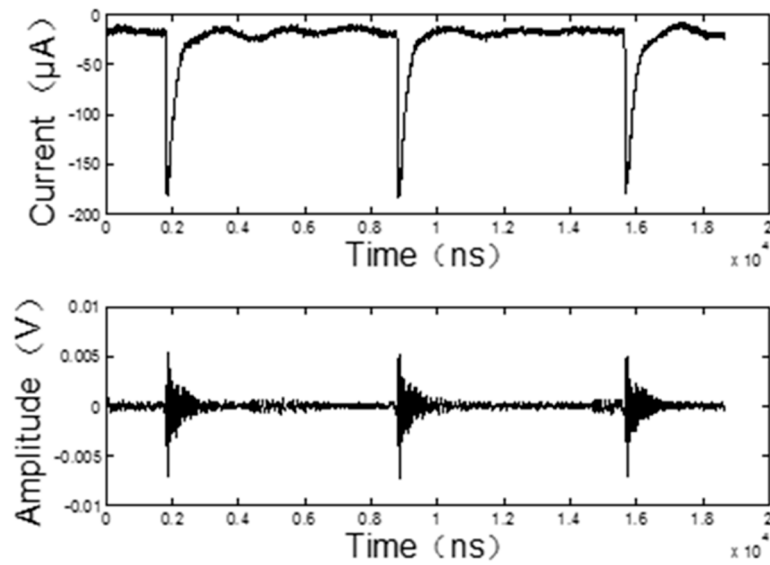
86 The signal detection module includes an oscilloscope (Tektronix MDO3104), a spectrum
 87 analyzer (Agilent E4447A), and a receiving antenna (Discone Antenna OX-08-02, 20 MHz to 1000
 88 MHz). The oscilloscope measures the voltage waveform on the sampling resistor to calculate the
 89 discharge current. The corona discharge EM radiation signal is received by the wide-band diskcone
 90 antenna, and the distance d between the antenna and the discharge device can be adjusted. The signal
 91 received by the antenna is analyzed by the spectrum analyzer, and the signal is collected by the
 92 oscilloscope. In order to eliminate the influence of external electromagnetic interference on the test
 93 results, all experiments were carried out in a microwave anechoic chamber.

94 3. Experimental Results and Analysis

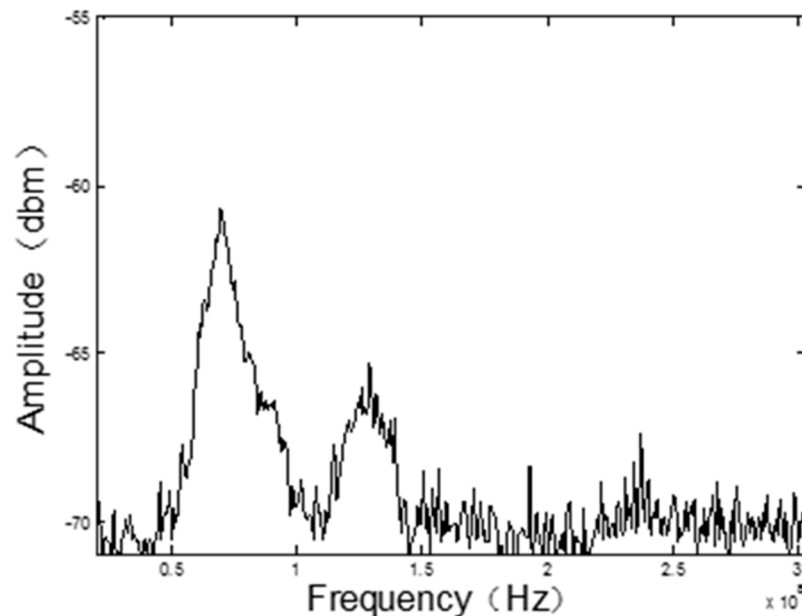
95 3.1. Single-Needle Negative Corona Discharge Trichel Pulse Current and Its Radiation Characteristics

96 The initial stage of negative corona discharge is the Townsend discharge stage, and the discharge
 97 current is usually within $1 \mu\text{A}$ and relatively stable. As the applied voltage increases, the discharge
 98 enters the Trichel pulse stage. Figure 2 shows the Trichel pulse current and its radiated signal
 99 waveform. Trichel pulses have a short rising time, which is typically tens of ns. The falling time is
 100 typically a few hundred ns, much larger than the rising time. Trichel pulses have a stable repetition
 101 rate. In the Trichel pulse stage, it will radiate electromagnetic waves to the surroundings. The
 102 waveform of the discharge radiation signal received by the antenna corresponds to the Trichel pulse
 103 current waveform. The repetition frequency of it is the same as the repetition frequency of the Trichel
 104 pulse current. Therefore, it is believed that the discharge radiation signal is generated by the Trichel
 105 pulse process. The spectrum of the discharge EM radiation signal under atmospheric pressure is
 106 shown in Figure 3. It can be seen from the figure that the spectrum of the single-needle discharge
 107 radiation signal is mainly within 200 MHz. The energy distribution near 70MHz is large (the
 108 fundamental frequency of the EM radiation signal), and there is also a certain energy distribution
 109 near 132 MHz. (second-harmonic generation of the EM radiation signal).

110



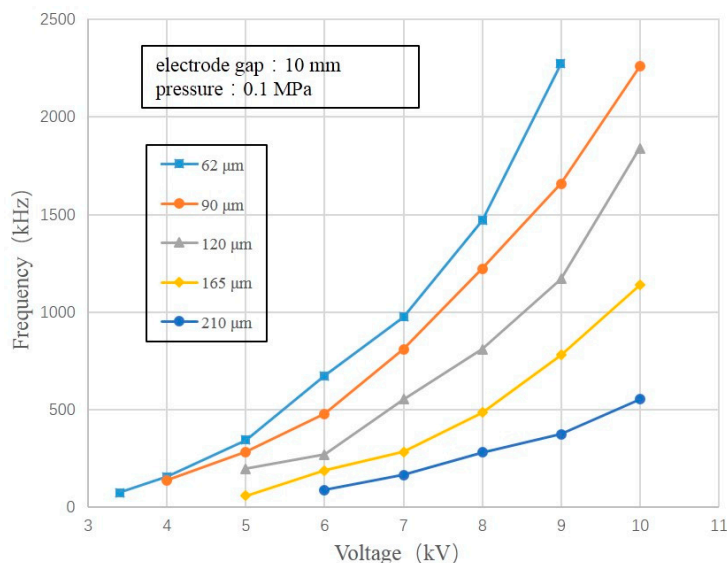
111 **Figure 2.** Trichel pulse current and its EM radiation signal



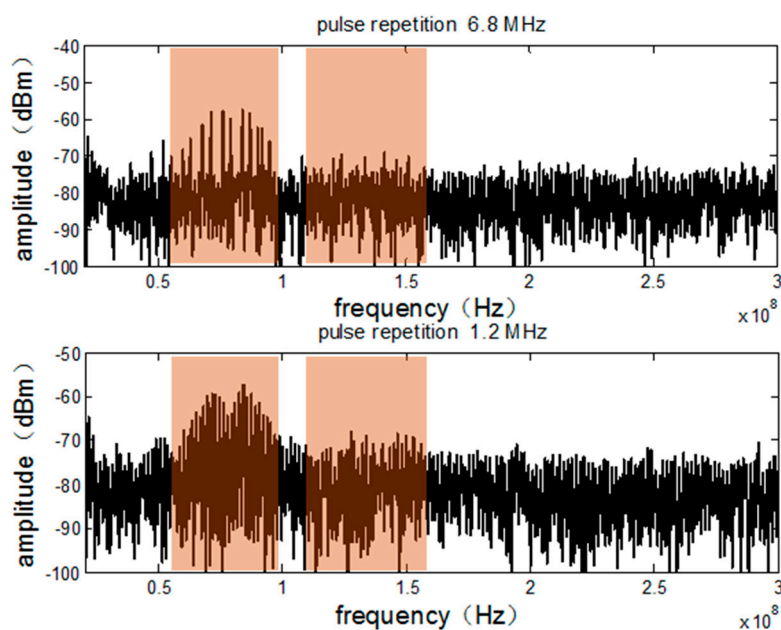
112 **Figure 3.** The spectrum of negative corona discharge EM radiation signal

113 The Trichel pulse generated by negative corona discharge is related to factors such as the applied
 114 voltage, the air pressure, and the tip radius of the discharge needle. Figure 4 shows the relationship
 115 between the repetition frequency of the Trichel pulse and the applied voltage. As the applied voltage
 116 increases, the repetition frequency of Trichel pulse increases, and the amplitude of a single pulse
 117 decreases slightly. This is consistent with the research results of Leob [19]. The spectrum of the
 118 discharge radiation signal at different pulse repetition frequencies is shown in Figure 5. The intensity
 119 of the discharge EM radiation signal decreases slightly, the frequency of the EM radiation signal does
 120 not change, the spectral lines become denser, and the average power of the discharge radiation signal
 121 increases as the increase of the repetition frequency of Trichel pulse current generated by the negative
 122 corona discharge. It is also found that changes in gap distance of electrode do not affect the intensity
 123 and frequency of the radiation signal.

124



125 **Figure 4.** The relationship between Trichel pulse repetition frequency and applied voltage



126 **Figure 5.** Spectrum of discharge radiation signal at different pulse repetition frequencies

127 As shown in Table 1, when the air pressure is reduced from 0.1 MPa to 0.04 MPa, the rising
 128 time of the Trichel pulse increases from 52 ns to 265 ns, while the pulse amplitude remains
 129 unchanged. Studies show that the discharge EM radiation signal spectrum is only related to the
 130 rising time of Trichel pulse[19]. The main frequency position of the EM radiation signal generated
 131 by the negative corona discharge shifts from 70 MHz to 45 MHz and the power of the discharge EM
 132 radiation signal decreases from 1.926 nW to 0.185 nW.

133 As the tip radius of the discharge needle increases from 62 μm to 210 μm, the amplitude of the
 134 Trichel pulse increases from 240 μA to 550 μA. And the rising and falling time of the pulse remains
 135 unchanged. This result is consistent with that of Lama[20] and Dordizadeh[21]. The frequency of the
 136 negative corona discharge electromagnetic radiation signal remains unchanged and the power of the
 137 radiation signal increases from 1.926 nW to 8.581 nW.

138

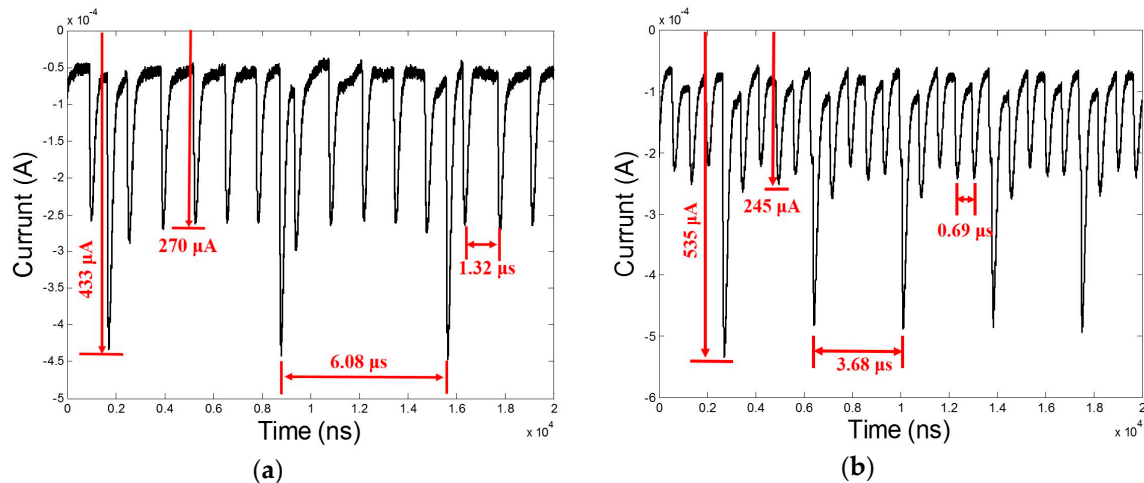
139
140**Table 1.** Negative corona discharge Trichel pulse current and its radiation characteristics under different tip radius and different air pressures.

Tip radius (μm)	Air pressure (MPa)	Pules amplitude (μA)	Rising time (ns)	Tip radius (μm)	Air pressure (MPa)
94	0.04	241	264	0.185	45,84
94	0.06	245	118	0.752	52,102
94	0.08	243	78	1.19	65,125
94	0.1	240	52	1.926	70,132
120	0.1	290	52	2.395	70,132
165	0.1	410	53	4.796	70,132

141 Therefore, the frequency of the single-needle negative corona discharge EM radiation signal will
 142 be determined when the air pressure is determined. The intensity of the EM radiation signal of the
 143 negative corona discharge is affected by the air pressure and the tip radius of cathode. The applied
 144 voltage and the gap distance of electrode have no effect on the EM radiation signal frequency, which
 145 only affect the intensity and the average power of the discharge radiation signal.

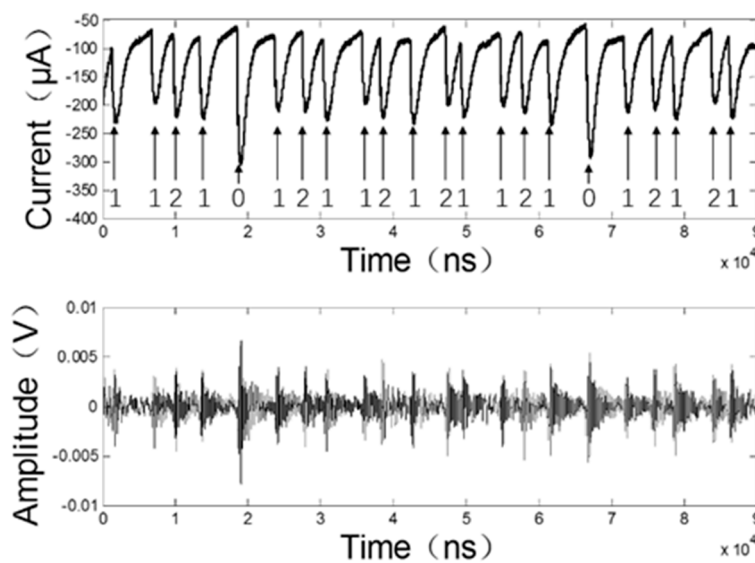
146 3.2. Multi-needle Negative Corona Discharge Characteristics

147 In practical applications, corona discharge often has a multi-needle (multi-point) structure. The
 148 waveform of a multi-needle discharge is significantly different from that of a single-needle discharge.
 149 We first tested the double-needle discharge Trichel pulse current. To distinguish the Trichel pulse
 150 currents generated by different discharge needles, we chose two discharge needles with tip radius of
 151 168 μm and 94 μm respectively for experiments (the larger the tip radius is, the larger the amplitude
 152 of the Trichel pulse current is). The discharge condition is: applied voltage of 7.4 kV, the gap distance
 153 of 10 mm, the ambient pressure of 0.1 MPa, and the relative humidity of 42%. The discharge current
 154 is shown in Figure 6a. It can be clearly seen from the figure that the amplitude of the Trichel pulse
 155 current generated by the discharge needle with a smaller radius is about 270 μA , and the pulse
 156 interval time is 1.32 μs . The amplitude of the Trichel pulse current generated by the large radius
 157 needle is about 440 μA , and the pulse interval time is 6.08 μs . Under this voltage, the Trichel pulse
 158 currents generated by the two discharge needles appear separately. Through further increasing the
 159 applied voltage, the discharge current waveform is shown in Figure 6 b. It can be seen from the figure
 160 that as the applied voltage increases, the amplitude of the Trichel pulse current generated by the
 161 smaller radius tip decreases from about 270 μA to about 245 μA , and the pulse interval time decreases
 162 to 0.69 μs . At the same time, it can be seen that when the applied voltage rises to a certain value, the
 163 Trichel pulses generated by the discharge needle with larger tip radius and smaller tip radius
 164 superimpose with each other. The maximum amplitude of the superimposed pulse current can reach
 165 535 μA . The minimum amplitude can also reach 490 μA , which is significantly larger than the
 166 unsuperimposed pulse. We also tested the discharge current of the multi-needle discharge structure.
 167 The test result is similar to the double-needle discharge. As the applied voltage increases, the smaller
 168 tip radius needle begins to discharge first. When the applied voltage is further increased, the other
 169 needles also begin to discharge. The Trichel pulse current between the needles occurs separately in a
 170 certain voltage range. However, as the applied voltage continues to increase, the Trichel pulse current
 171 generated by the different discharge needles will be superimposed, and the amplitude of the
 172 superimposed pulse will increase significantly.



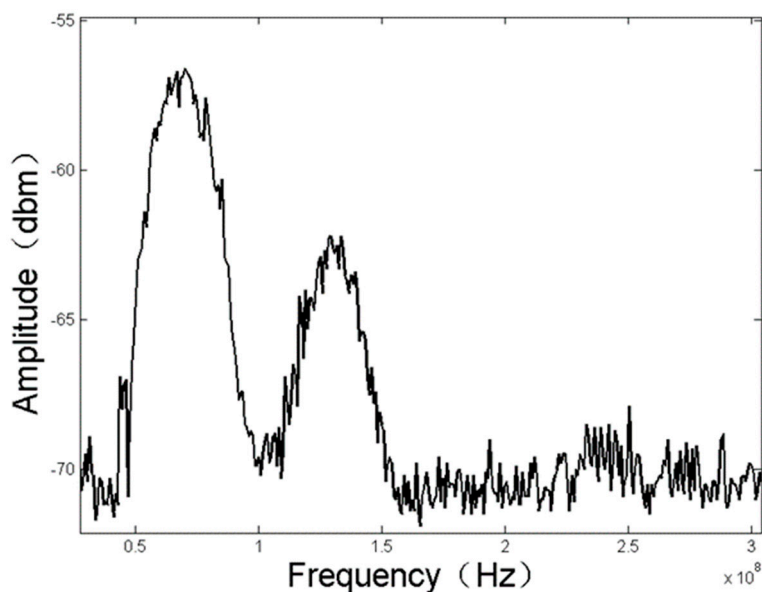
173 **Figure 6.** Negative corona discharge current waveform under double-needle discharge structure: (a)
 174 Applied voltage of 7.4 kV; (b) Applied voltage of 8.7 kV

175 When the applied voltage is lower, the Trichel pulse processes of the two needles will not happen
 176 at the same time. The EM radiation signal generated by the negative corona discharge corresponds
 177 to the Trichel pulse current, so the EM radiation signal is determined by the Trichel pulse current
 178 generated by each needle. When the applied voltage rises to an appropriate value, the Trichel pulse
 179 processes of the two needles will occur simultaneously. The Trichel pulse current waveform and the
 180 EM field signal generated during the simultaneous discharge of the two needles are shown in Fig. 7.
 181 The pulse pointed by the arrow 1 and the arrow 2 is the Trichel pulse generated by the two different
 182 discharge needles respectively, and the larger pulse pointed by the arrow 0 is the superimposed pulse
 183 generated by the simultaneous discharge of the two discharge needles. It can be seen that the
 184 discharge radiation signal generated by the non-superimposed Trichel pulse current has an
 185 amplitude of about 4.5 mV, and for the superimposed pulse current, the amplitude of the generated
 186 EM radiation signal can reach 7.5 mV. Therefore, when the double-needle simultaneous discharge
 187 pulse currents superimpose, the generated EM radiation field will also be superimposed, and the EM
 188 radiation signal intensity will increase significantly.



189
 190 **Figure 7.** Trichel pulse current and radiation signal of the double-needle discharge structure

191



192 **Figure 8.** Spectrum of discharge radiation signal of the double-needle discharge structure

193 The double-needle discharge radiation spectrum is shown in Figure 8. The air pressure is 0.1
 194 MPa, and the tip radius of both discharge needles is 60 μm . It can be seen that the spectrum of the
 195 EM radiation signal of the double-needle negative corona discharge is mainly distributed within
 196 200 MHz, the signal intensity is large in the frequency band around 70 MHz, and there is also a
 197 certain spectrum distribution in the frequency band around 140 MHz. Under the same discharge
 198 condition, the double-needle negative corona discharge has the same frequency as the single-needle
 199 negative corona discharge. However, when the Trichel pulse processes of two discharge needles
 200 occur simultaneously, the spectral intensity of the generated EM radiation signal increases
 201 significantly when the pulse process is superimposed, and the spectral intensity of the radiation
 202 signal near 70 MHz is increased from -60 dBm of the single-needle discharge structure to -57 dBm
 203 of the double-needle discharge structure.

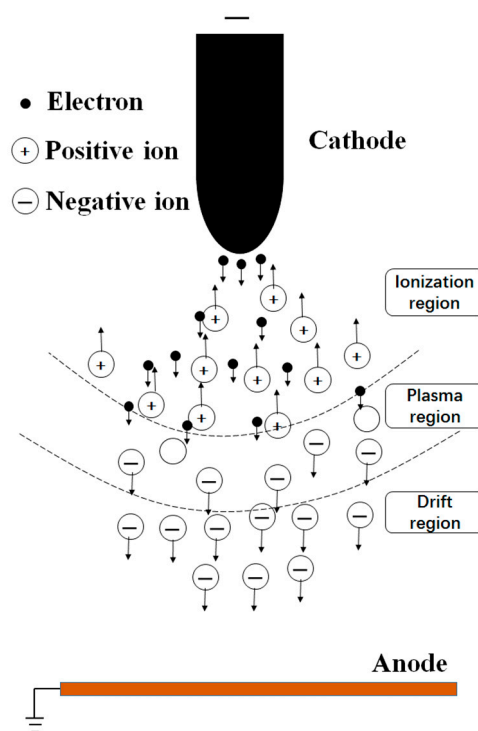
204 The frequency of the EM radiation signal generated by the double-needle negative corona
 205 discharge is only related to the ambient pressure. When the air pressure is determined, the
 206 frequency of the radiation signal generated by the double-needle discharge will remain unchanged.
 207 The intensity of the EM radiation signal is related to the air pressure, the tip radius of cathode and
 208 applied voltage.

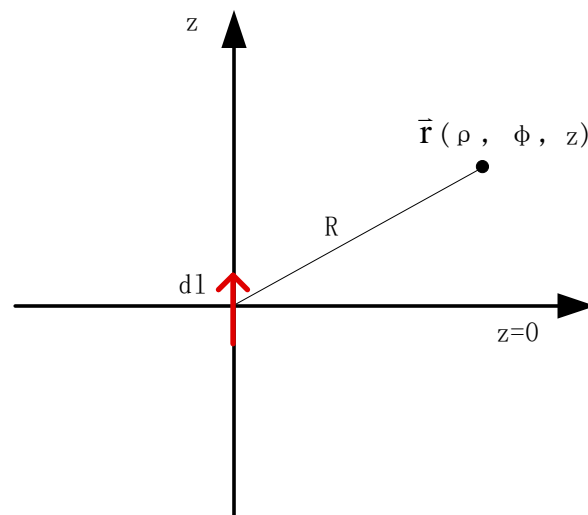
209 It is found through the experimental test that the multi-needle simultaneous discharge current
 210 characteristics and EM radiation characteristics are basically consistent with those of the double-
 211 needle discharge structure. When the applied voltage is low, the pulse processes of the discharge
 212 needles do not occur at the same time, and the radiation signals are generated by the discharge pulse
 213 process of each discharge needle alone. As the applied voltage rises, different discharge needle pulse
 214 processes may occur simultaneously, and the pulse currents will be linearly superimposed, resulting
 215 in an increase in the discharge radiation field intensity. If the applied voltage is increased
 216 continuously, the corona discharge will enter the glow stage, the discharge current will be in a DC
 217 state, and the radiation signal will disappear. The frequency of the EM radiation signal of the multi-
 218 needle negative corona discharge is only related to the air pressure. The number of discharge needles,
 219 the tip radius of cathode, the gap distance of electrode and the applied voltage only affect the intensity
 220 of the discharge radiation signal. Therefore, when the air pressure is determined, the frequency of
 221 the EM radiation signal will also be determined, and the detection of the negative corona discharge
 222 can be realized by detecting the characteristic spectrum of the negative corona discharge radiation
 223 signal.

224

225 **4. Discussion**226 *4.1. Mechanism Analysis of EM Radiation Generated by Negative Corona Discharge*

227 The space between the two electrodes of negative corona discharge can be divided into a
 228 ionization zone, a plasma zone and a drift zone[22]. As shown in Figure 9. The ionization region is
 229 near the tip of the discharge needle. At the beginning of the discharge, the seed electrons near the
 230 electrode collide with the neutral air molecules under the action of a strong electric field. The neutral
 231 molecules are ionized into positive ions and electrons, the positive ions move toward the negative
 232 electrode under the action of the electric field, and the electrons continue to ionize other neutral
 233 molecules under the action of the electric field. In a very short period of time, the number of electrons
 234 increases sharply, forming an ionosphere near the tip of the discharge needle, and the external circuit
 235 current increases sharply. This process is called electronic avalanche. The thickness of the ionization
 236 region of the negative corona discharge is usually about 1.5 mm[1]. Since the electric field is relatively
 237 strong and the charge-to-mass ratio of the electron is relatively large in this region, the velocity of
 238 electrons in this region can reach 0.01 times the speed of light[23,24]. After leaving the ionization
 239 region, the electrons will enter the plasma region. The electric field in the plasma region cannot
 240 provide sufficient energy for the electrons to complete the impact ionization. Therefore, the electrons
 241 combine with the neutral air molecules to form negative ions in the plasma region, and then enter
 242 into the drift region and move towards the anode under the action of the electric field. Since the
 243 charge-to-mass ratio of positive ions and negative ions is much larger than that of electrons,
 244 the velocity of positive ions and negative ions is negligible compared to electrons moving at high speed
 245 in the ionization region. Therefore, it can be considered that for each pulse process in the entire
 246 discharge region, the discharge EM radiation field is generated due to the exponential growth and
 247 rapid movement of electrons in the process of the electron avalanche in the ionization region and the
 248 plasma region.

249 **Figure 9.** Negative corona discharge region division



250 **Figure 10.** Negative corona discharge dipole radiation model

251 We equate the EM radiation field generated by negative corona discharge to the dipole radiation
 252 model, as shown in Figure 10. The dipole length $dl=1.5\text{mm}$ (thickness of the ionization region), the
 253 direction is along the z -axis of the cylindrical coordinates, and the center of the dipole is the
 254 coordinate origin. For this configuration, the fields are found to be:

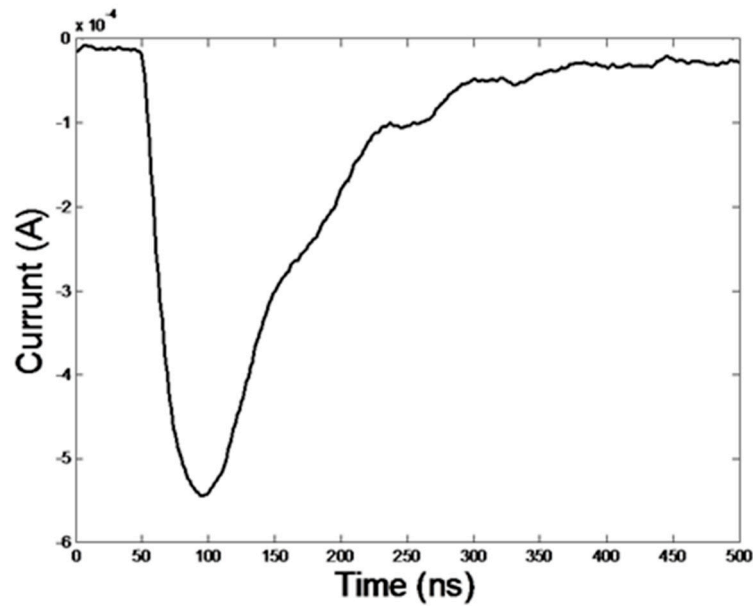
$$\begin{aligned} \vec{E}(\vec{r}, t) &= \bar{a}_\rho dl \frac{\eta_0 \rho z}{2\pi R^2} \left\{ \frac{3i(u)}{R^2} + \frac{1}{cR} \frac{\partial i(u)}{\partial u} \right\} + \bar{a}_z dl \frac{\eta_0}{2\pi} \left\{ \left[\frac{3z^2}{R^2} - 1 \right] \frac{i(u)}{R^2} + \left[\frac{z^2}{R^2} - 1 \right] \frac{1}{cR} \frac{\partial i(u)}{\partial u} \right\} \\ H(\vec{r}, t) &= \bar{a}_\phi dl \frac{1}{2\pi R} \left\{ \frac{i(u)}{R^2} + \frac{1}{cR} \frac{\partial i(u)}{\partial u} \right\} \end{aligned} \quad (1)$$

255 Where R the distance from the discharge point to the observation point $\vec{r}(\rho, \phi, z)$, η_0 the free
 256 space wave impedance, $i(u)$ the discharge current time-dependent waveform evaluated at time u ,
 257 where $u = t - R/c$ indicates the time lag when the radiation signal propagates to point P .

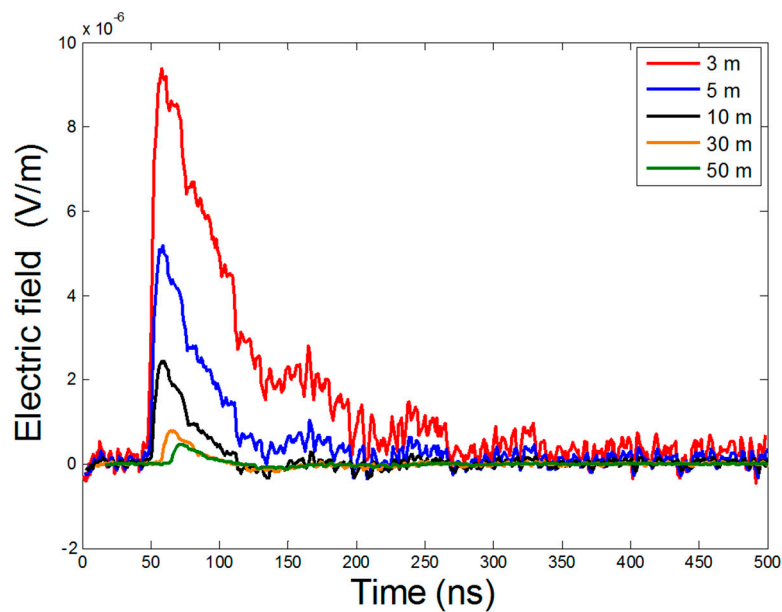
258 According to equation (1), the space around the discharge needle can be divided into a near-
 259 field region ($d < \lambda/2\pi$) and a far-field region ($d > \lambda/2\pi$), where λ is the wavelength of the
 260 radiation signal[25]. In the near-field region, the EM radiation signal is mainly determined by $i(u)$.
 261 The intensity of the radiation signal is attenuated as R^2 . In the far field, the EM radiation signal is
 262 mainly determined by $\partial i(u)/\partial t$, and the EM radiation signal intensity is attenuated as R .

263 Substitute the experimentally measured Trichel pulse current into the dipole radiation model to
 264 calculate the EM radiation field generated by the Trichel pulse. Figure 11 shows the Trichel pulse
 265 current of the discharge needle with a tip radius of $210\mu\text{m}$ under 0.1MPa . The current amplitude is
 266 $550\mu\text{A}$, and the rising time is 53ns .

267 Substitute the Trichel pulse current into equation (1) to calculate the discharge radiation field
 268 intensity waveform at different detection distances. As shown in Figure 12, the calculated EM
 269 radiation field intensity forms a pulse form, and the amplitude of the radiation signal is
 270 approximately inversely proportional to the detection distance. The electromagnetic wave
 271 propagates in the space at the speed of light, and the EM radiation field delay time is different at
 272 different positions.



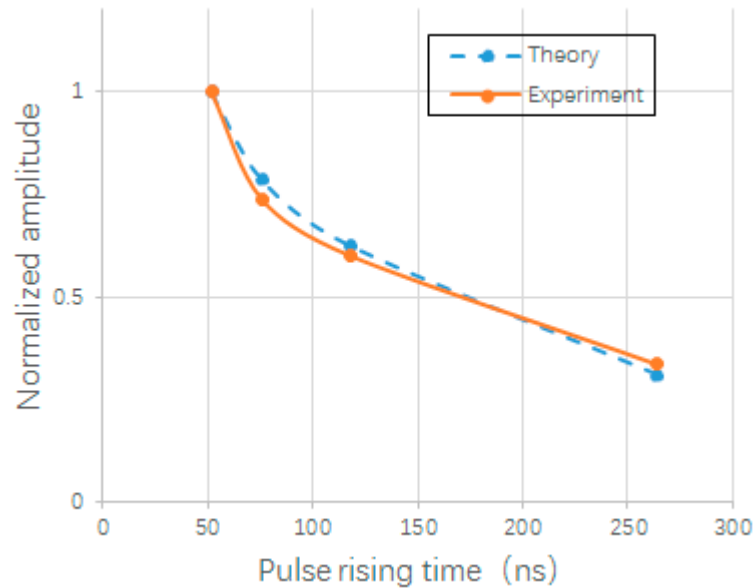
273 **Figure 11.** Single Trichel pulse current waveform



274 **Figure 12.** Discharge EM radiation field waveform

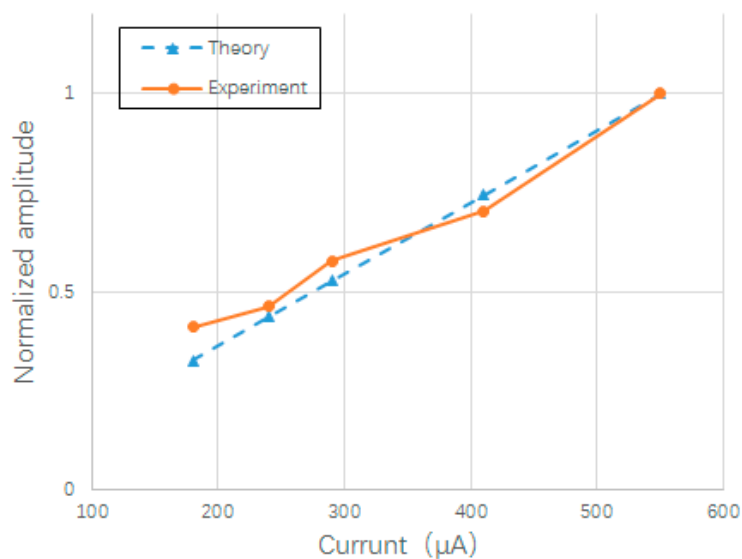
275 4.2. Comparison of Calculation Results of Dipole Radiation Model with Experimental Test Results

276 Document [18] has studied the effect of Trichel pulse current parameters on the discharge
 277 radiation spectrum. This paper mainly analyzes the relationship between the amplitude of discharge
 278 EM radiation field and Trichel pulse parameters. When the single Trichel pulse current waveform is
 279 the same, as the pulse repetition frequency increases, the average power of the radiation signal will
 280 increase, but the repetition frequency of the pulse will not affect the EM radiation signal generated
 281 by each pulse current, which is consistent with the experimental results (Figure 5).



282
283

Figure 13. Theoretical calculated and experimentally tested "relationship between Trichel pulse rising edge and radiation signal amplitude"



284
285

Figure 14. Theoretical calculated and experimentally tested "relationship between Trichel pulse amplitude and radiation signal amplitude"

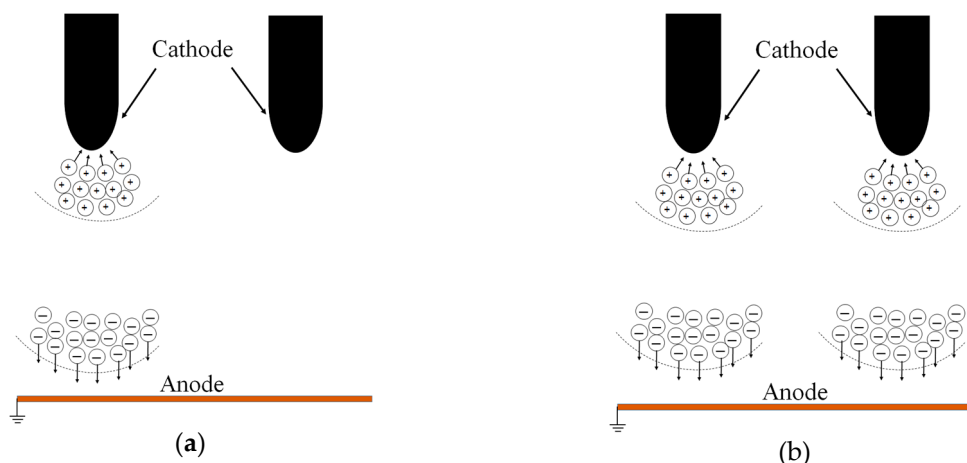
286
287
288
289
290
291
292
293
294
295
296
297

The band of the antenna used in the experimental test is 20 MHz~1000 MHz. When the antenna was placed at a distance of 3m from the discharge device, the received radiation signal shows far-field characteristics. The discharge EM radiation signal was dominated by $\partial i(u) / \partial t$. If the $\partial i(u) / \partial t$ becomes smaller, the amplitude of the EM radiation signal will be smaller. As the air pressure decreases, the rising time of the Trichel pulse becomes larger, and other parameters of the Trichel pulse remain unchanged. As shown in Figure 13, when the rising time of the pulse increases from 52 ns to 264 ns, the amplitude of the theoretically calculated EM radiation signal decreases by 69%, and the amplitude of the experimentally tested EM radiation signal decreases by about 66%. The theoretical and experimental results were basically consistent. When the tip radius of the cathode increases, the amplitude of the Trichel pulse increases, and other parameters of the Trichel pulse remain unchanged. When the amplitude of the Trichel pulse increases from 180 μA to 550 μA , the $\partial i(u) / \partial t$ increases, the intensity of the EM radiation signal increases, as shown in Figure 14. The

298 theoretically calculated amplitude of the radiation signal increases approximately linearly, and the
 299 measured value is consistent with the theoretical value.

300 4.3. Effects of Multi-Needle Discharge Structure on EM Radiation Characteristics of Negative Corona 301 Discharge

302 The ionization during negative corona discharge generates a large number of electrons and
 303 positive ions in the ionization region. Since the charge-to-mass ratio of electrons is much smaller than
 304 that of ions, the ions move slowly in the electric field and form positive ion clouds in the ionization
 305 region. The electrons leave the ionization region during the movement to the anode and combine
 306 with the neutral particles to form negative ions, forming a negative ion cloud outside the ionization
 307 region. The space charge of the positive ion cloud and the negative ion cloud will generate a spatial
 308 electric field, which has an effect on the original electric field[26]. In the multi-needle discharge
 309 structure, the ion cloud formed by the discharge needle in the pulse phase will affect the electric field
 310 around the nearby discharge needle, thereby affecting the Trichel pulse process. As shown in Figure
 311 15, when a discharge needle is subjected to a pulse process, the positive ion cloud formed by it has
 312 little effects on the electric field in the ionization direction of the other discharge needle, and the
 313 negative ion cloud has a significant weakening effect on the electric field in the ionization direction
 314 of the other discharge needle. Therefore, in the case of a small applied voltage, the previous discharge
 315 needle pulse process has an inhibitory effect on the other discharge needle pulse process[27]. As the
 316 applied voltage increases, the effect of the negative ion cloud is reduced, and the pulse processes of
 317 the two discharge needles occur simultaneously.



318 **Figure 15.** Double-needle Trichel pulse process: (a) Trichel pulse process under small applied voltage;
 319 (b) Trichel pulse process under large applied voltage.

320 5. Conclusions

321 In this paper, the pulse current characteristics of multi-needle negative corona discharge and its
 322 EM radiation characteristics are studied.

323 In the multi-needle discharge structure, when the applied voltage is low, the negative corona
 324 discharge Trichel pulse processes of the respective discharge needles are mutually suppressed, and
 325 the discharge needle pulse processes occur separately. When the applied voltage increases to a certain
 326 threshold, the pulse processes of different discharge needles will occur simultaneously, the multi-
 327 needle discharge current will be linearly superimposed, and the generated EM radiation field will
 328 also be linearly superimposed. The frequency of the radiation signal after multi-needle simultaneous
 329 discharge superposition is the same as the frequency of the single-needle discharge EM radiation
 330 signal, but the amplitude of the EM radiation signal is increased.

331 The negative corona discharge radiation process can be equivalent to the dipole antenna
 332 radiation model. The dipole length is the sum of the thickness of the ionization region and the plasma
 333 region. The radiation field in the near-field region is dominated by $i(u)$, and the discharge radiation

334 field in the far-field region is dominated by $\partial i(u)/\partial t$. The amplitude of the EM radiation signal is
335 related to the tip radius of the cathode and the air pressure. The larger the tip radius, the larger the
336 amplitude of the pulse current, and the larger the intensity of the EM radiation signal. The lower the
337 air pressure, the larger the rising time of the pulse, the smaller the change of current as time, and the
338 smaller the intensity of the radiation signal. The spectral characteristics of the EM radiation of the
339 multi-needle negative corona discharge are only related to the air pressure. The intensity of the EM
340 radiation signal is related to the tip radius of the cathode, the air pressure, and the number of
341 discharge needles.

342 The results of this work may provide promising method for evaluation of insulation condition
343 of electric apparatus as well as detection of the charged body.

344 **Author Contributions:** Conceptualization, C.W. and X.C.; Methodology, C.W. and J.O; Software, C.W. and J.F.;
345 Validation, C.W , J.O. and X.C. ; formal analysis, C.W. and J.F ; Investigation, J.O.; Resources, C.W. and X.C.;
346 Data curation, C.W. and X.C.; Writing—original draft preparation, C.W. and X.C.; Writing—review and editing,
347 C.W.; Visualization, C.W.; Supervision, X.C.; Project administration, X.C.; Funding acquisition, C.W , X.C. and
348 J.O.;"

349 **Funding:** This work was financially supported by grants from National Natural Science Foundation of China
350 (#U1630130, #51777010, #51707008, #51407009).

351 **Conflicts of Interest:** The authors declare no conflict of interest.

352

353 **References**

- 354 1. Rycroft, M. J. Gas discharge physics. *J. Atmos. Terr. Phys.* **1993**, *55*, 1487, doi:10.1016/0021-
355 9169(93)90114-E.
- 356 2. Sigmond, R. S. *Corona Discharges*; 1978;
- 357 3. Bussiahn, R.; Brandenburg, R.; Gerling, T.; Kindel, E.; Lange, H.; Lembke, N.; Weltmann, K. D.; Von
358 Woedtke, T.; Kocher, T. The hairline plasma: An intermittent negative dc-corona discharge at
359 atmospheric pressure for plasma medical applications. *Appl. Phys. Lett.* **2010**, *96*, doi:10.1063/1.3380811.
- 360 4. Kanazawa, S.; Chang, J. S.; Round, G. F.; Sheng, G.; Ohkubo, T.; Nomoto, Y.; Adachi, T. Removal of
361 NO_x from flue gas by corona discharge activated methane radical showers. *J. Electrostat.* **1997**, *40–41*,
362 651–656, doi:10.1016/S0304-3886(97)00072-7.
- 363 5. Pongráč, B.; Kim, H. H.; Janda, M.; Martišovič, V.; Machala, Z. Fast imaging of intermittent
364 electrospraying of water with positive corona discharge. *J. Phys. D: Appl. Phys.* **2014**, *47*,
365 doi:10.1088/0022-3727/47/31/315202.
- 366 6. Jaworek, A.; Krupa, A. Electrical characteristics of a corona discharge reactor of multipoint-to-plane
367 geometry. *Czechoslov. J. Phys.* **1995**, *45*, 1035–1047, doi:10.1007/BF01691996.
- 368 7. Huang, S.; Liu, Y.; Chen, S.; Zhou, G.; Zhuang, W. Corona Onset Characteristics of Bundle Conductors
369 in UHV AC Power Lines at 2200 m Altitude. *Energies* **2018**, doi:10.3390/en11051047.
- 370 8. Abdel-Salam, M.; Hashem, A.; Sidique, E. Characteristics of negative corona discharge in single-
371 needle- and multi-needle-to-plane configurations. *Int. J. Plasma Environ. Sci. Technol.* **2013**, *7*, 121–135.
- 372 9. Tanner, R. L.; Nanevicz, J. E. An Analysis of Corona-Generated Interference in Aircraft. *Proc. IEEE*
373 **1964**, *52*, 44–52, doi:10.1109/PROC.1964.2741.
- 374 10. El-Khabiry, S.; Colver, G. M. Drag reduction by dc corona discharge along an electrically conductive
375 flat plate for small Reynolds number flow. *Phys. Fluids* **1997**, *9*, 587–599, doi:10.1063/1.869219.
- 376 11. Thanh, L. C. Negative Corona in a Multiple Interacting Point-to-Plane Gap in Air. *IEEE Trans. Ind.*
377 *Appl.* **1985**, *IA-21*, 518–522, doi:10.1109/TIA.1985.349697.
- 378 12. Trichel, G. W. The mechanism of the negative point to plane corona near onset. *Phys. Rev.* **1938**, *54*,
379 1078–1084, doi:10.1103/PhysRev.54.1078.
- 380 13. Fernando, S. C. Electromagnetic Radiation due to Partial Discharge and Fault Detection Method for
381 Overhead Distribution Lines Electromagnetic Radiation due to Partial Discharge and Fault Detection
382 Method for Overhead Distribution Lines. **2012**, 1–118.
- 383 14. Zhang, L.; Han, X.; Li, J. Partial discharge detection and analysis of needle-plane defect in SF₆ under
384 negative oscillating lightning impulse voltage based on UHF method. *IEEE Trans. Dielectr. Electr. Insul.*
385 **2017**, *24*, 296–303, doi:10.1109/TDEI.2016.005979.
- 386 15. Juette G W, Charbonneau H, Dobson H I, et al. CIGRE/IEEE survey on extra high voltage
387 transmission line radio noise. *IEEE Trans. Power Appar. Syst.* **1973**, *PAS-92*, 1019–1028,
388 doi:10.1109/TPAS.1973.293668.
- 389 16. Nayak, S. K.; Thomas, M. J. A Novel Technique for the Computation of Radiated EM1 due to Corona
390 on HV Transmission Lines. 738–742.
- 391 17. Tsutsumi Yasuyuki et al. Electromagnetic noise spectra of corona discharge at point-to-plane
392 electrodes in air. *IEEJ Trans. Fundam. Mater.* **2008**, *111*, 733–740.
- 393 18. Zhang, Y.; Liu, L. J.; Miao, J. S.; Peng, Z. L.; Ouyang, J. T. Trichel pulse in negative DC corona
394 discharge and its electromagnetic radiations. *J. Electr. Eng. Technol.* **2015**, *10*, 1174–1180,
395 doi:10.5370/JEET.2015.10.3.1174.

- 396 19. Loeb, L. B.; Kip, A. F.; Hudson, G. G.; Bennett, W. H. Pulses in negative point-to-plane corona. *Phys.*
397 *Rev.* **1941**, *60*, 714–722, doi:10.1103/PhysRev.60.714.
- 398 20. Lama, W. L.; Gallo, C. F. Systematic study of the electrical characteristics of the “trichel” current pulses
399 from negative needle-to-plane coronas. *J. Appl. Phys.* **1974**, *45*, 103–113, doi:10.1063/1.1662943.
- 400 21. Dordizadeh, P.; Adamiak, K.; Castle, G. S. P. Experimental study of the characteristics of Trichel pulses
401 in the needle-plane negative corona discharge in atmospheric air. *J. Electrostat.* **2017**, *88*, 49–54,
402 doi:10.1016/j.elstat.2016.12.013.
- 403 22. Chen, J.; Davidson, J. H. Model of the Negative DC Corona Plasma: Comparison to the Positive DC
404 Corona Plasma. *Plasma Chem. Plasma Process.* **2003**, *23*, 83–102, doi:10.1023/A:1022468803203.
- 405 23. Nath, D.; Kumar, U. Total electric field due to an isolated electron avalanche. *IEEE Trans. Dielectr.*
406 *Electr. Insul.* **2016**, *23*, 2562–2571, doi:10.1109/TDEI.2016.005593.
- 407 24. Cooray, V.; Cooray, G. Electromagnetic radiation field of an electron avalanche. *Atmos. Res.* **2012**, *117*,
408 18–27, doi:10.1016/j.atmosres.2011.06.004.
- 409 25. Wilson, P. F.; Ma, M. T. Fields Radiated by Electrostatic Discharges. *IEEE Trans. Electromagn. Compat.*
410 **1991**, *33*, 10–18, doi:10.1109/15.68245.
- 411 26. Colver, G. M.; El-Khabiry, S. Modeling of DC corona discharge along an electrically conductive flat
412 plate with gas flow. *IEEE Trans. Ind. Appl.* **1999**, *35*, 387–394, doi:10.1109/28.753633.
- 413 27. Lama, W. L.; Gallo, C. F. Interaction of the “trichel” current pulses of a pair of negative coronas. *J. Phys.*
414 *D. Appl. Phys.* **1973**, *6*, 1963–1972, doi:10.1088/0022-3727/6/16/317.